

Lawrence Berkeley National Laboratory

LBL Publications

Title

THE STRUCTURE OF Rh(III) (2x2)-3CO FROM LEED INTENSITIES: SIMULTANEOUS BRIDGE AND NEAR-TOP ADSORPTION IN A DISTORTED COMPACT HEXAGONAL CO OVERTAYER

Permalink

<https://escholarship.org/uc/item/1972r3s4>

Author

Hove, M.A. Van

Publication Date

1982-12-01



Lawrence Berkeley Laboratory

UNIVERSITY OF CALIFORNIA

Materials & Molecular Research Division

RECEIVED
LAWRENCE
BERKELEY LABORATORY

APR 15 1983

LIBRARY AND
DOCUMENTS SECTION

Submitted to Surface Science

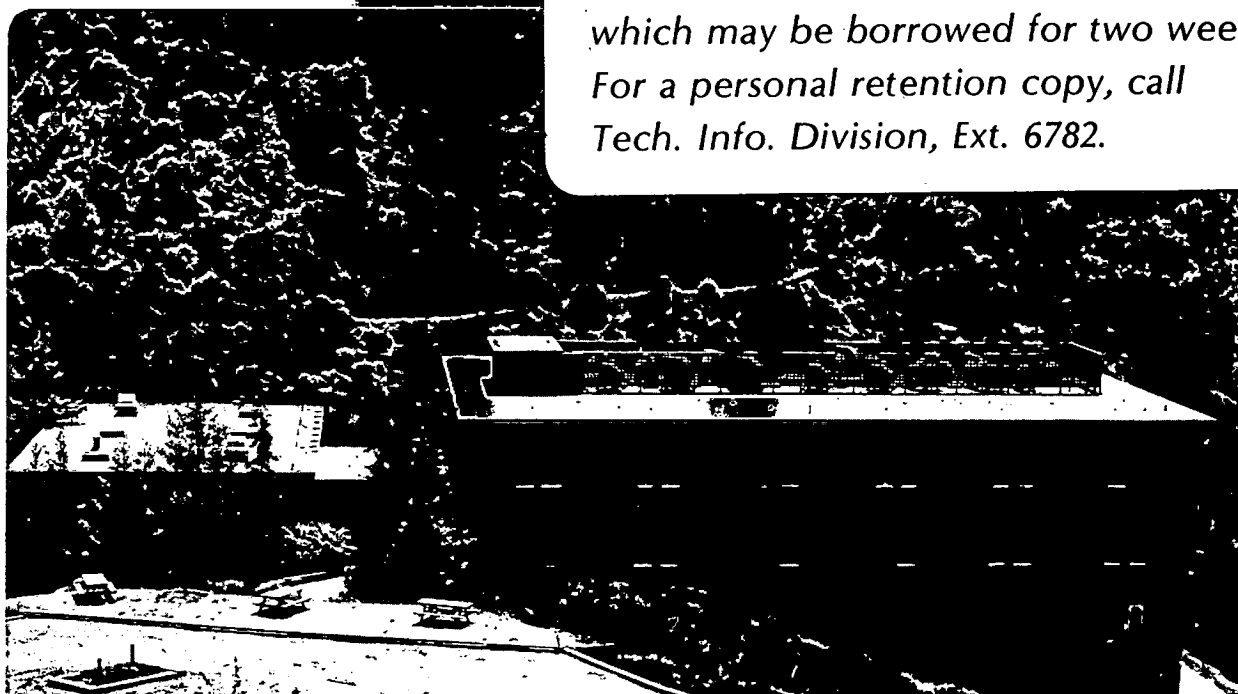
THE STRUCTURE OF Rh(111) (2x2)-3CO FROM LEED
INTENSITIES: SIMULTANEOUS BRIDGE AND NEAR-TOP
ADSORPTION IN A DISTORTED COMPACT HEXAGONAL
CO OVERLAYER

M.A. Van Hove, R.J. Koestner, J.C. Frost,
and G.A. Somorjai

December 1982

TWO-WEEK LOAN COPY

*This is a Library Circulating Copy
which may be borrowed for two weeks.
For a personal retention copy, call
Tech. Info. Division, Ext. 6782.*



LBL-15271
c. 2

DISCLAIMER

This document was prepared as an account of work sponsored by the United States Government. While this document is believed to contain correct information, neither the United States Government nor any agency thereof, nor the Regents of the University of California, nor any of their employees, makes any warranty, express or implied, or assumes any legal responsibility for the accuracy, completeness, or usefulness of any information, apparatus, product, or process disclosed, or represents that its use would not infringe privately owned rights. Reference herein to any specific commercial product, process, or service by its trade name, trademark, manufacturer, or otherwise, does not necessarily constitute or imply its endorsement, recommendation, or favoring by the United States Government or any agency thereof, or the Regents of the University of California. The views and opinions of authors expressed herein do not necessarily state or reflect those of the United States Government or any agency thereof or the Regents of the University of California.

THE STRUCTURE OF Rh(111) (2x2)-3CO FROM LEED INTENSITIES: SIMULTANEOUS
BRIDGE AND NEAR-TOP ADSORPTION IN A DISTORTED COMPACT HEXAGONAL CO OVERLAYER

M.A. Van Hove, R.J. Koestner, J.C. Frost* and G.A. Somorjai

Materials and Molecular Research Division
Lawrence Berkeley Laboratory

and

Department of Chemistry
University of California
Berkeley, California 94720

ABSTRACT

The first Low-Energy Electron Diffraction (LEED) intensity analysis of molecular adsorption in multiple sites is presented. A 3/4 monolayer CO overlayer on Rh(111) is found to involve one bridge site and two near-top sites in each unit cell, which supports the bridge and top assignment based on earlier High-Resolution Electron Energy Loss Spectroscopy (HREELS) data. The near-top site is asymmetrical, with the CO axis close to the surface normal (but possibly tilted about 5°), yielding a bent Rh-C-O species. The near-top CO molecules are forced sideways from the ideal top site by ~ 0.53Å due to bridge-bonded CO molecules located at a distance of 2.85Å. This short CO-CO separation is somewhat smaller than corresponding intermolecular separations found in metal carbonyl clusters and crystalline CO and CO₂. The resulting CO overlayer has a hexagonal geometry that is distorted both parallel and perpendicular to the surface due to the strong metal-CO bonding. The Zanazzi-Jona and Pendry R-factors for the best structure are 0.25 and 0.47, respectively.

* Permanent address: Dept. of Chemistry, Heriot-Watt University, Riccarton, Currie, Edinburgh, Scotland.

The LEED analysis exhibits the use of different levels of approximation in the multiple scattering theory in order to show the value of approximate but fast calculations in preliminary structural searches.

A new algorithm to obtain experimental I-V curves from digitized images of LEED patterns is described.

1. INTRODUCTION

The adsorption of carbon monoxide on single-crystal transition metal surfaces has received considerable attention⁽¹⁾ by the surface science community. Not only can the chemisorption of CO on a metal surface be regarded as a model adsorption system but its industrial importance is great in such areas as the catalysis of CO hydrogenation⁽²⁾ to produce hydrocarbons and of CO oxidation⁽³⁾ in controlling automobile exhaust.

Studies by Low-Energy Electron Diffraction (LEED),⁽⁴⁾ Thermal Desorption Spectroscopy (TDS),⁽⁵⁾ Ultraviolet Photoemission Spectroscopy (UPS)⁽¹⁾ and the vibration-sensitive techniques of Infrared Spectroscopy (IR)⁽⁶⁾ and High-Resolution Electron Energy Loss Spectroscopy (HREELS)⁽⁷⁾ indicate significant differences in the CO bonding to the various transition and noble metal surfaces and for different crystal faces, notably in the choice of adsorption site. Apart from those cases where the molecules dissociate, the CO species can occupy top, bridge and possibly also hollow sites in various ordered or disordered arrangements at coverages up to about 1/3 or 1/2 monolayers. At higher coverages, the molecules often adsorb simultaneously in different kinds of sites. The structure of the higher-coverage CO layers is under debate and will be discussed in light of our present study: a compressed hexagonal CO lattice has been proposed for many surfaces, but ordered domain structures generally agree

better with all observations.

In the hope of obtaining a more detailed picture of the bonding of CO to metal surfaces, we have studied the ordered overlayer structures of the CO/Rh(111) system by LEED crystallography. We found⁽⁸⁾ that CO stands above the top sites in the low-coverage ($\theta = 1/3$) structure $(\sqrt{3} \times \sqrt{3})R30^\circ$, in agreement with results of an earlier HREELS investigation.⁽⁷⁾ In this paper we report an investigation of the (2×2) structure obtained at high coverage ($\theta = 3/4$). HREELS studies indicate the presence of two types of CO molecules on the Rh(111) surface when this structure is observed by LEED. We hope to demonstrate that LEED can be successfully applied to a molecular overlayer which contains two or three CO molecules per unit cell, two of which are structurally inequivalent, occupying both top and bridge sites.

Until now, LEED crystallography has been applied to only a few CO overlayers and each of these involved only one adsorption site: top site for Ni(100) $c(2 \times 2)$ -CO,⁽⁹⁻¹¹⁾ Cu(100) $c(2 \times 2)$ -CO⁽⁹⁾ and Rh(111) $(\sqrt{3} \times \sqrt{3})R30^\circ$ -CO,⁽⁸⁾ and bridge site for Pd(100) $(2/2 \times 2)R45^\circ$ -2CO.⁽¹²⁾

This structural determination provides a necessary check and also a calibration on the rule originally proposed by Eischens and Pliskin,⁽¹³⁾ according to which the measured C-O stretching frequency is related to either top, bridge or hollow site adsorption. (Top site adsorption is assigned to frequencies above about 2000 cm^{-1} , bridge site adsorption to frequencies between about 2000 and 1850 cm^{-1} and hollow site adsorption to frequencies below about 1850 cm^{-1} .) This is because the three frequency ranges assigned to three adsorption sites are not well separated from each other, and more generally because various other factors can strongly influence the observed frequencies (electronic effects in the metal-CO bond, direct and indirect CO-CO interactions, image charge effects, etc.).

The relative importance of adsorbate-adsorbate and metal-adsorbate interactions can also be examined in this structure determination. If metal-adsorbate interactions dominate, CO should stand directly above high-symmetry sites; however, if adsorbate-adsorbate interactions are significant, the CO overlayer would relax into a more hexagonal arrangement unrelated to the substrate lattice.

A correspondingly larger computational effort is required in this study than in previous cases where there are fewer atoms per unit cell. Therefore, we adopt a three-stage approach involving different levels of approximation in the LEED theory, each more accurate but less efficient than the preceding one. In the process, we exhibit the value of this approach which efficiently weeds out unpromising structural models and permits rapid refinement of the more promising ones.

2. EXPERIMENTAL

The rhodium crystal (> 99.9% purity) was mounted on a manipulator that allowed both polar (θ) and azimuthal (ϕ) rotations. The vacuum system is equipped with four-grid LEED/Auger optics, a glancing incidence Auger electron gun, and a mass spectrometer head; the base pressure remained at $\sim 1 \times 10^{-9}$ torr during these experiments, H_2 and CO being the major ambient gases. As reported earlier,⁽⁸⁾ the Rh(111) sample was cleaned by repeated Ar^+ bombardments (1-3 amps, 1.2 kV) with five minute annealing at 800°C and O_2 treatments (flowing 5×10^{-7} torr O_2 , 700°C); Auger electron spectra revealed small S, C, B and Cl contamination after cleaning (see Figure 4 in reference 8).

As the CO exposure and coverage increase, a series of ordered structures form on the Rh(111) surface; the progression of patterns^(5,14) is a fuzzy (2×2) at $\theta = 1/4$, $(\sqrt{3} \times \sqrt{3})R30^\circ$ at $\theta = 1/3$, a "split" (2×2) for $1/3 < \theta < 3/4$, and a (2×2) pattern at $\theta = 3/4$. The order-order transition from the "split"

(2x2) to the (2x2) structure is reversible with respect to ambient CO pressure and crystal temperatures. Near 300K a background pressure of 10^{-6} - 10^{-5} torr CO is necessary to maintain the (2x2) overlayer; however, if the crystal temperature is raised to 325K, even the 10^{-5} torr of ambient CO is not sufficient to produce the (2x2) structure.⁽⁵⁾ In our experiments, the (2x2) layer was formed by cooling the sample to 240K and exposing it to a constant pressure of $2-4 \times 10^{-6}$ torr CO. This steady state pressure was maintained by using a small leak rate and throttling the ion pump.

The CO molecules are known not to dissociate appreciably,⁽¹⁴⁾ while the CO coverage was determined to be about 3/4 of a monolayer by our AES measurements and by TDS experiments.⁽¹⁴⁾ The choice of one or two molecules per (2x2) unit cell is, therefore, unreasonable. A structure with four molecules per (2x2) unit cell (one monolayer) is also unreasonable, for several reasons: one would then expect a (1x1) structure which is not observed; it is known to be difficult to pack CO so densely (the Rh-Rh distance along the surface is 2.68\AA , whereas CO diameters perpendicular to the CO axis are most likely rather larger than that, as will be discussed in Section 5); and two different adsorption sites appear in HREELS, which in view of the molecular size is incompatible with a (1x1) structure. This leaves the only option of three molecules per unit cell, giving a coverage of 3/4.

The diffraction beam intensities for the Rh(111) (2x2)-3CO structure were obtained by the photographic technique.^(15,16) A Beattie Varitron view camera (fitted with a Bencher external shutter and an 85mm, f1.8 Nikon lens) was adjusted for the maximum aperture and a 1/2 sec exposure time; the diffraction intensities were recorded on a high-speed Kodak film (Panchromatic 2484). The photographs, taken at 2 eV increments, were digitized with a scanning microdensitometer and then analyzed with a new computer program to give the desired

intensity vs. voltage (I-V) curves. The algorithm used in this program is described in the Appendix. For use in a reliability factor analysis, the I-V spectra were averaged over degenerate beams and independent runs, normalized to a 1μamp incident beam current, and smoothed twice with a three-point formula.

Intensity data were collected at three different incidence angles and a second independent experiment was performed at each angle to check the reproducibility. The data set contains five independent beams at normal incidence ($\theta = 0^\circ$), eight independent beams at $\theta = 10^\circ$, $\phi = 0^\circ$ and eight independent beams at $\theta = 20^\circ$, $\phi = 0^\circ$; these intensity curves are available on request in either digitized or plotted form. As reported in our earlier Rh(111)($\sqrt{3}\times\sqrt{3}$)R30°-CO structure determination,⁽⁸⁾ electron beam damage to the (2x2)-3CO overlayer was minimized by moving the sample during the course of photography; as a result, the electron exposure at any given region of the sample did not exceed 40μamp-sec. It was found that the initial decay rate of the (0, 1/2) beam intensity with electron exposure was about one tenth as large as that measured for the (1/3, 1/3) beam in the Rh(111)($\sqrt{3}\times\sqrt{3}$)R30°-CO or the (0, 1/2) beam in the Rh(111)(2x2)-C₂H₃ overlayer. This suggests that electron-beam induced desorption of CO is more probable than decomposition and that the background pressure of CO needed to produce the (2x2) structure may also fill any vacancies due to desorption. In agreement with this explanation, an AES study⁽¹⁷⁾ of CO on Pt(111) reported that the cross-section (at ~ 200 eV) for electron-impact desorption is about ten times larger than the cross-section for dissociation.

3. THEORETICAL METHODS

The basic theoretical methods⁽¹⁸⁾ used for the structural determination described here are similar to those that we have applied in other recent studies

of molecular overlayers on Rh(111).^(8,16) In particular, all the non-structural parameters are identical to those used for the Rh(111)($\sqrt{3}\times\sqrt{3}$)R30°-CO surface structure. The structural complexity of the present molecular overlayer necessitated the use of the Combined Space Method^(18a) (spherical waves within the overlayer, plane waves between layers). This method increases the required computing effort markedly, which motivated the use of more efficient approximations.

The Rh(111)(2x2)-3CO surface, in fact, was found to be a good candidate to explore the value of performing the structural search in three different stages of increasing accuracy and decreasing computing efficiency, as introduced in recent model calculations applied to a surface composed of benzene-like C₆ rings.^(18b) In the first stage, we ignore all multiple scattering within the overlayer, whose unit cell contains three CO molecules and, therefore, six atoms; the kinematic reflection and transmission matrices for all beams diffracted by this layer are then used to obtain the reflectivity of the entire surface by Renormalized Forward Scattering (RFS),^(18a) thereby including all multiple scattering within the substrate and between the substrate and the overlayer. In the next stage, multiple scattering is included between the closely-spaced C and O atoms of the same molecule, but not between different CO molecules, since they are separated by larger distances which reduces the likelihood of multiple scattering. This is achieved by a version of the Reverse Scattering Perturbation (RSP) method,⁽¹⁸⁾ in which the Green's function propagators are made to vanish between atoms more separated than a suitable cutoff distance. The third stage includes all multiple scattering, brought to convergence in the conventional RSP scheme,⁽¹⁸⁾ and is in that sense exact.

To explore the relative merit of these three levels of accuracy, we have applied each in turn to essentially the same sets of structural models for

Rh(111)(2x2)-3CO. In the future, our approach will be to apply the kinematic stage of calculations to a large number of a priori reasonable model structures. On the basis of their performance as compared to experiment, we shall reduce the number of plausible models. Then the next more accurate stage of computations would be used to further restrict and refine the search among the more promising structures, while performing the final selection and refinement with full multiple scattering calculations.

In this work we have adopted the scheme of scanning the various structural parameters in pairs over fairly wide ranges (for example varying one bond length and one bond angle simultaneously), producing two-dimensional cross-sections through the N-dimensional structural parameter space; such scans allow one to make progressively better guesses for the various parameters, using an R-factor as a measure of the agreement between theory and experiment.⁽¹⁹⁾ An alternative approach would have been, for example, to make a first structural guess and search for the best structure by the method of steepest descent or least squares,⁽¹⁹⁾ again using an R-factor.

We apply the same R-factors that were used in our previous work,^(8,16) namely five R-factors with different definitions as well as their average. The search is conducted on the basis of this average R-factor, while we also quote some individual R-factors^(20,21) for the preferred structure.

4. STRUCTURAL SEARCH AND RESULTS

First, structural models must be proposed for the Rh(111)(2x2)-3CO system. The substrate is assumed bulk-like, since the clean surface is bulk-like to within the LEED accuracy.⁽⁸⁾ The 3/4 monolayer coverage is compatible with a close-packed hexagonal lattice, cf. Figure 1, in which the Rh(111) substrate fixes the CO-CO distances at about 3.10Å. This distance corresponds well with

similar distances inferred from saturation coverage of CO on other metal surfaces based on a compressed hexagonal packing.(6,22)

HREELS detects for this surface two adsorption sites that are most likely top sites and bridge sites.(7b) The HREELS peak ratio for these two sites is about 1.5:1, which is qualitatively comparable to a 2:1 occupation of top and bridge sites. This feature and the hexagonal arrangement favor the basic structural model shown in Figure 1. This puts 2/3 of the molecules in "near-top" sites. Other "registries" (lateral displacements of the overlayer) would place some of the molecules in 3-fold coordinated hollow sites, incompatible with HREELS results, or produce unsatisfactory lower-symmetry arrangements, which we cannot exclude but do not consider in this work, since the model of Figure 1 proves very successful.

With the registry shown in Figure 1 there is one mirror plane perpendicular to the surface, which is used as a projection plane in the upper part of Figure 1. If one ignores the second and deeper metal layers, there is an additional mirror plane perpendicular to the first one that makes all bridge-site molecules perpendicular to the surface and all near-top molecules equivalent to each other. Even with adsorbates that are more strongly bonded to the surface than CO, the asymmetry in the second and deeper metal layers is generally believed to have a very small effect, and we shall, therefore, assume that this symmetry plane exists for the overlayer structure. Thus, the number of independent structural parameters is reduced to six. Another assumption in our work will be that all CO bond lengths on this surface are equal. This is justified, since the apparent uncertainty in determining this bond length by LEED(8,10-12) is larger than the actual variations of the CO bond length from one site to another, as indicated from structural determinations of metal carbonyl clusters.(23) Thus, we are left with five independent structural parameters: $d_{\perp RhC}$, d_{CO} , $d_{\perp CC}$, $d_{//CC}$

and θ_{CO} , defined in Figure 1. Their variations in our structural search are summarized in Table 1: in the three levels of approximation, starting with the kinematic limit, the numbers of structures investigated were approximately 150, 120 and 250, respectively.

We present the results of our structural search in the form of selected R-factor contour plots (the five-R-factor average is used). Each plot is obtained by varying two structural parameters; in each case one of the two parameters is the metal-overlayer distance, whose variation is relatively cost-effective in the computation compared to the variation of a parameter internal to the overlayer structure itself. (18a) The experimental data base used in this analysis consists of the five independent beams measured at normal incidence: (10) , (01) , $(\frac{1}{2}, 0)$, $(\frac{1}{2}, \frac{1}{2}) = (0, \frac{1}{2})$ and $(\frac{1}{2}, \frac{1}{2})$.

Figure 2 shows R-factor contour plots based on the kinematic approximation within the molecular overlayer, all independent structural parameters being varied. It is significant that all parameter variations produce a clear minimum in the R-factor at values that are reasonable in terms of bond lengths and bond angles. If the guessed structures were grossly wrong, one could not expect this to occur: there would be ill-defined minima, or no minima, or minima at unreasonable locations. In addition, the best agreement between theoretical and experimental I-V curves is already very encouraging.

Figure 3 shows corresponding R-factors when multiple scattering within the individual molecules is included. The best agreement has improved noticeably after this inclusion, despite a reduction of the number of phase shifts used from eight to six. Again the minima occur at reasonable locations that are consistent with those of Figure 2. The minimum in the d_{CC} variation has split up into two minima: this is the largest change that we have observed in varying the level of approximation in the calculation; presumably the use

of a larger data base would have avoided this splitting. This splitting, in fact, disappears with the "exact" calculation, cf. Figure 4. The full-multiple-scattering calculation again produces minima in the same regions, and the best R-factor values have generally decreased slightly again, although not as much as before, since the newly included multiple scattering between molecules is relatively weak.

These examples indicate the usefulness of applying the kinematic approximation in the search for a molecular structure: the R-factor minima in our case shift by less than 0.1\AA and 0.5\AA for atomic movements perpendicular and parallel to the surface, respectively. The parallel movement considered here is probably a worst case, in which two opposing motions occur whose contributions to the diffraction tend to cancel each other out in the lowest approximation.

The computing times for the three levels of approximation scaled as 1:3:7.5, where the quickest approximation used eight phase shifts throughout the surface, compared to six phase shifts for the other two.

It was found that the best R-factor value could be improved by reducing the value of $d_{//CC}$ from 3.10\AA (corresponding to an hexagonal CO layer) to about 2.85\AA , while the other parameters keep the values shown explicitly in Figures 2-4. Some R-factors with full multiple scattering are indicated in Figure 5, which constitute our best results. The best average R-factor value becomes 0.19, while the corresponding Zanazzi-Jona and Pendry R-factor values are 0.25 and 0.47, respectively. The three comparable R-factor values for our determination of the $\text{Rh}(111)(\sqrt{3}\times\sqrt{3})R30^\circ\text{-CO}$ structure⁽⁸⁾ are 0.23, 0.40 and 0.50, respectively; thus, the present study appears to have achieved a better agreement between theory and experiment (for further comparison, the best Pendry R-factor values for $\text{Ni}(100)c(2\times 2)\text{-CO}$ and $\text{Cu}(100)c(2\times 2)\text{-CO}$ are 0.50 and 0.40, respectively⁽⁹⁾). Some representative I-V curves near the optimum geometry are shown in Figure 6.

The optimized structural parameter values are: $d_{\perp RhC} = 1.52 \pm 0.1\text{\AA}$, $d_{\perp CC} = 0.35 \pm 0.1\text{\AA}$, $d_{CO} = 1.15 \pm 0.1\text{\AA}$, $d_{\parallel CC} = 2.85 \pm 0.2\text{\AA}$, $\theta_{CO} = -5 \pm 15^\circ$. Here the quoted uncertainties are based on the contour levels of Figure 6, using for calibration an uncertainty of 0.1\AA in layer spacings, which may be somewhat conservative. The optimum structure is illustrated in Figure 1 with $\theta_{CO} = 0^\circ$. We obtain a CO lattice that is distorted from an hexagonal arrangement in three ways: by a displacement of the near-top CO molecules in the direction closer to the ideal top sites, by a buckling of the layer in response to the different adsorption sites and by a possible small tilting of the near-top molecules away from the nearest neighboring molecules and towards the linear Rh-C-O configuration.

5. DISCUSSION

Adsorption Site

Our optimum structure for Rh(111)(2x2)-3CO, illustrated in Figure 1, confirms the simultaneous occupation by CO of both the bridge and top sites predicted by HREELS, although we prefer to speak here of "near-top" sites. We thus show that the CO stretch frequency for an asymmetrical near-top site (2070 cm^{-1}) can still fall in the conventional range assigned⁽¹³⁾ to top sites ($2000\text{--}2150\text{ cm}^{-1}$). Presumably, a shift occurs in the CO stretch frequency due to the asymmetrical siting: this shift would be additional to the shift usually encountered with increasing coverage (visible for example in the coverage range below $1/3$ for CO on Rh(111)(7b)). As there is no qualitative difference in the frequency shifts observed below and above $1/3$ monolayer for CO on Rh(111), we conclude that the shift due to asymmetrical location of the CO molecules is not greater than that due to other coverage-dependent effects.

This structure constitutes the fifth CO adsorption structure for which LEED has confirmed the correlation between CO vibrational frequencies and adsorption site.⁽⁸⁻¹²⁾ It is the first that involves simultaneously two different sites and the first that involves an asymmetrical site (near-top).

The asymmetry of each near-top site might produce a detectable metal-CO bending mode in HREELS (expected near the metal-CO stretch frequency), but this was not unambiguously observed: it could have overlapped with one of the two metal-CO stretch frequencies or it was too weak. It is of interest to compare the 2:1 relative occupation of near-top and bridge sites with the relative HREELS peak heights at the corresponding CO stretch frequencies: after rough deconvolution the HREELS peak heights have a ratio of about 1.5:1. Thus, the bridge-site CO molecules appear to have a dynamic dipole about 4/3 times that of near-top molecules, but this assumes that all other effects involved in the HREELS process are site-independent.

Bond Lengths

The optimal Rh-C bond lengths that we find are $1.94 \pm 0.1\text{\AA}$ and $2.03 \pm 0.07\text{\AA}$ for the near-top and bridge sites, respectively. These values, together with the $1.15 \pm 0.1\text{\AA}$ CO bond lengths, are compared in Figure 7 with the previous LEED results for CO bond lengths when adsorbed on metal surfaces⁽⁸⁻¹²⁾ and with bond length values in metal carbonyl clusters⁽²³⁾ (to allow comparison between different metals, the bulk metal radius has been subtracted from the metal-C distances). Although one should bear in mind the relatively large uncertainties of the LEED results, the M-C and C-O bond lengths found for surfaces fall within the ranges found for the M-C and C-O bond lengths in clusters for the appropriate bonding site (top bridge or hollow). Figure 7 exhibits a few interesting correlations, especially among the more accurate cluster results, which lead us to speculate on the mechanism of CO chemisorption.

The metal-C and C-O bond lengths tend to vary, for a given metal, in opposite directions: a smaller metal-C distance corresponds to a larger C-O distance, which presumably reflects a complementarity between a strengthening metal-C bond and a weakening C-O bond. Furthermore, from top to bridge to hollow site there is an increase in both the metal-C and the C-O bond lengths. Although the longer metal-C distance would indicate a weaker bond, the multiplicity of such bonds can produce an overall stronger substrate-molecule bond, and this is reflected by a lengthened C-O distance due to a possibly weaker C-O bond (however, high-coordination metal-carbon bonds for CO are sometimes observed to be weaker than low-coordination ones, as is the case for the present system Rh(111)(2x2)-3CO⁽⁵⁾). These trends are in general agreement with the mechanism of CO chemisorption proposed by Blyholder,⁽²⁴⁾ which involves backdonation of electronic charge from the metal into a molecular orbital that is antibonding between C and O but bonding between the metal and C. It also appears that more backdonation tends to favor a higher-coordination site.

CO Tilting

We now discuss the orientation of the CO molecular axes with respect to the surface normal. Apart from small asymmetrical effects due to the deeper metal layers, the bridge-site CO molecules can be assumed to be essentially perpendicular to the surface (certainly within the present uncertainty of LEED). But the near-top molecules could try to retain linear bonding in a tilted orientation while at the same time also trying to remain perpendicular to the surface due in part to crowding by neighboring molecules. The observed tilt angle of $5 \pm 15^\circ$ is too uncertain to lead to a definite conclusion, but it is at least in the expected direction towards linear bonding and away from the nearest CO neighbors.

There are indications⁽²⁵⁾ from Angle-Resolved UPS studies, that a fraction of the CO molecules in the Pt(100)_c(4x2)-3CO surface structure is tilted by 10 to 15° from the surface normal. We shall return to this result in connection with a discussion of the CO-CO intermolecular distances.

Intermolecular Distances

Of special interest are the CO-CO distances in densely packed CO overlayers. They help understand the relative importance of site-preference due to strong metal-CO bonding and of intermolecular forces. A weak site-preference would favor a planar CO layer that is hexagonally close-packed, comparable to incommensurate layers of adsorbed rare gases. On the other hand, a strong site preference would position molecules as close as possible to the ideal high-symmetry sites and induce a strong buckling in the layer whenever different sites are involved. Our results show that both tendencies are detectable for CO on Rh(111) and they are of the same magnitude: there is a strong site-preference but also a strong repulsive CO-CO interaction at the spacings occurring here. Moreover, our result gives a good estimate of how close CO molecules can approach each other on a surface. As Figure 1 shows, a given near-top molecule has one nearest neighbor at a distance of 2.85Å and two next-nearest neighbors at a distance of 2.88Å, other neighbors lying 3.23 and 3.60Å away (these distances are measured in the surface plane, ignoring the CO layer buckling and any CO tilting). Since a high background pressure of CO is required to maintain this (2x2) surface structure, we can say that in less extreme cases of crowding the closest CO-CO spacing should be somewhat larger than 2.85Å.

We may compare this situation with the recent ARUPS results⁽²⁵⁾ for Pt(100)_c(4x2)-3CO, in which some CO molecules appear to be tilted by 10 to 15° from the surface normal. A model for this surface,⁽²⁶⁾ based on high-symmetry

sites (either two top sites and one bridge site per unit cell or vice versa) and antiphase domains, produces some CO-CO distances that are equal to the metal-metal distance, i.e. 2.77Å. Maximum relaxation of the CO centers towards a hexagonal lattice by tilting of linear Pt-C-O species in the more likely two-top/one-bridge configuration would imply a CO tilt of about 10° from the surface normal and minimum CO-CO distances of about 3.33Å. Thus, the ARUPS prediction of a 10-15° tilt on Pt(100) and our 2.85Å minimum CO-CO separation for a more closely-packed layer on Rh(111) appear to be quite compatible.

The smallest comparable CO-CO distances that we have found reported for clusters are as follows. In syn-1,6:8,13-biscarbonyl[14]annulene⁽²⁷⁾ two CO's are bridge-bonded across a 14-carbon ring with CO axes diverging by 21°: the C-C and O-O distances between the carbonyls are 2.72 and 3.17Å, respectively, giving an average of 2.96Å. In the three molecules $[(CO)_4M-P(CH_3)_2]_2$, with M = V, Cr and Mn,⁽²⁸⁾ there are pairs of nearly parallel carbonyls linearly bonded to two metal atoms, the metal-metal distances being 2.73, 2.90 and 3.67Å, respectively: the C-C (O-O) distances in the three molecules are 3.18 (3.40)Å, 3.03 (3.22)Å and 3.54 (3.46)Å, respectively, giving averages of 3.29, 3.12 and 3.50 Å for the center-center separations, while the CO axes diverge from each other by 11.1°, 9.5° and -4.1°, respectively (the CO axes converge slightly for M = Mn).

Finally, we compare the CO/Rh(111) overlayer with three-dimensional molecular crystals⁽²⁹⁾ of CO and CO₂. No plane in these crystals yields a close-packed arrangement of molecules oriented perpendicularly to that plane, so that no direct comparison with our overlayer is possible. But it remains of interest to compare interatomic distances with the 2.85Å found in the dense overlayer on Rh(111). In the cubic α-CO crystal, with a CO bond length of 1.06 ± 0.01Å, any C or O atom has near neighbors in other molecules at distances of 3.46Å (C-O),

3.57Å (C-C and O-O) and 3.69Å (C-O). In the cubic CO₂ crystal, which has linear OCO molecules and a CO bond length of about 1.07Å, one finds interatomic distances between near molecules of 3.17Å (C-O), 3.23Å (O-O) and 3.98Å (C-C).

From these various comparisons it appears that CO molecules are somewhat more tightly packed when held together in a (2x2) structure on the Rh(111) substrate than in clusters and in three-dimensional CO or CO₂ crystals.

Our determination of the intermolecular CO distances is important in understanding the ordered structures that dense CO layers adopt on a variety of low-Millerindex metal surfaces. Two basic models are used to interpret the observed LEED patterns: (22,26) 1) compressed hexagonal CO layers, corresponding to weak site-preference (in occasional contradiction with IR and HREELS which indicate a strong site-preference); 2) ordered anti-phase domain structures in which domains of simple site-dominated structures join at misfit boundaries of high density requiring CO molecules to adsorb at about intermetallic distances from each other (typical intermetallic distances at fcc surfaces range from 2.49Å for Ni to 2.78 Å for Pt). In a number of cases these two models are equivalent after minor relaxations in CO positions, as is the case for Rh(111)(2x2)-3CO, but in others they are mutually exclusive, cf. Fig. 8.

The major objection to the second model (site-dominated) has been the need for small separations between CO molecules. However, our results on Rh(111) indicate that such distances are perfectly acceptable: CO molecules can apparently be positioned about 2.85Å or slightly more apart with only a small tilt away from each other. This allows CO molecules to occupy neighboring equivalent sites, such as two neighboring top sites, as required by the ordered domain model and by experimental evidence obtained by IR and HREELS.

The same issue of antiphase vs. compressed hexagonal structures has recently been analyzed for the system Pb/Cu(100): there, a $c(5\sqrt{2} \times 2)R45^\circ$ structure is

found at "high" coverage of Pb ($\theta = 0.6$), which was shown by LEED intensity calculations to have an antiphase arrangement of $c(2 \times 2)$ domains⁽³⁰⁾. At $\theta = 0.5$ a $c(2 \times 2)$ structure extends over the entire surface; at $\theta = 0.6$ strips of $c(2 \times 2)$ structure are separated by higher-density domain boundaries, similar to the arrangement shown in Fig. 8.

6. SUMMARY AND CONCLUSION

We have analyzed the geometric structure of $\text{Rh}(111)(2 \times 2)-3\text{CO}$, which is found to consist of a close-packed nearly hexagonal lattice of CO molecules. The departure from an hexagonal array is due to preference for CO adsorption in bridge and top sites. One of the three molecules in the (2×2) unit cell chooses a bridge site, where it is bound with its C-O axis perpendicular to the surface with Rh-C and C-O bond lengths of $2.03 \pm 0.07 \text{ \AA}$ and $1.15 \pm 0.1 \text{ \AA}$, respectively. The two other molecules are bound near top sites, $0.53 \pm 0.2 \text{ \AA}$ sideways from the ideal top site, and $0.25 \pm 0.2 \text{ \AA}$ away from the location that one would predict for a hexagonal CO layer; these molecules have Rh-C and C-O bond lengths of $1.94 \pm 0.1 \text{ \AA}$ and $1.15 \pm 0.1 \text{ \AA}$, respectively, producing a CO layer buckling of 0.35 \AA , as shown in Figure 1. Each near-top CO molecule may be slightly bent away from the linear Rh-C-O configuration and away from the nearest CO neighbor, which is located at a distance of $2.85 \pm 0.2 \text{ \AA}$: the CO tilt angle is $5 \pm 15^\circ$ from the surface normal. The minimum CO-CO distance found on $\text{Rh}(111)$ appears to be slightly shorter than the corresponding distances in carbonyl-containing clusters or in CO and CO_2 crystals. The best R-factor values are: 0.19 for our five-R-factor average, 0.25 for the Zanazzi-Jona R-factor and 0.47 for the Pendry R-factor.

The structural analysis employed LEED intensity calculations in which

three levels of approximation were compared for structural determination of complex surface structures. It was found that the crudest approximation (neglect of all multiple scattering within the molecular overlayer) yields a valuable, cost-efficient method for searching through a priori plausible surface structures and for reducing the number of likely structures to be tested by more accurate approximations. The intermediate-level approximation (restricted multiple scattering within the molecular overlayer) provides an additional stage of selection in the structural search. The most accurate calculations (including all multiple scattering) enable the structural parameters to be determined with a precision comparable to that found for simpler structures.

APPENDIX. An algorithm to obtain I-V curves from digitized pictures of LEED patterns.

In the photographic method that we use to acquire LEED I-V curves, one photographs the diffraction pattern visible on a conventional phosphor display screen at regular intervals (2 eV) over a wide range of incident beam energies. The photographic negatives are subsequently digitized using a microdensitometer for processing by a computer. In this Appendix, we describe a reliable algorithm for the automatic processing of the digitized data.

This algorithm supersedes one that has been used previously in this laboratory.⁽³¹⁾ In the previous algorithm, the 256 x 256 pixels of a frame were searched by computer for transmission minima (corresponding to bright spots) and a punched card was produced for each minimum, giving the integrated intensity and position of that spot. The cards were then carefully sorted manually to eliminate spurious minima (i.e. those unrelated to diffraction features, but due to noise or dust on the film) and to form for each beam sets

of cards at sequential energies. This process is slow, tedious and error-prone. A serious drawback is that a threshold intensity level must be established, which is significantly above the film background level and below which a minimum is ignored (otherwise, minor fluctuations in background levels cause cumbersome numbers of cards to be produced). The threshold generates gaps in the I-V profiles where the beam intensity falls below the limit. Such gaps make the increasingly important R-factor calculations difficult.(19)

The program described below eliminates these problems and only requires some final checking of the I-V curves to avoid erroneous results in the case of excessive noise.

A.1 Outline of the method.

The LEED display screen provides a view of the diffracted beams which is an almost undistorted representation of their positions in reciprocal space, cf. Fig. 9. By defining appropriate primitive unit cell vectors \vec{a} and \vec{b} to describe the LEED pattern, we can predict the position $(h\vec{a}, k\vec{b})$ on the screen of any diffraction beam with indices (h, k) ; the length of the vectors \vec{a} and \vec{b} of course depends on the incident energy E . We obtain values for the x and y components of \vec{a} and \vec{b} in the frame of the photographic negative together with an origin (O_x, O_y) by fitting these quantities to the positions of three or more strong diffraction spots on the film (the origin O normally corresponds to the specular spot, which may not be visible in a given experiment). Knowledge of \vec{a} , \vec{b} and O allows the positions of weak spots to be found and an intensity measurement to be made even when the spot intensity is zero or close to zero. The magnitudes of the cell vectors are proportional to the square root of the energy and so the spot positions can be predicted at the next energy, i.e. on the next photograph. This cycle can be continued until a complete set of

I-V profiles is obtained.

In practice, there are a number of complications which must be taken into account when designing an efficient algorithm to obtain I-V profiles. These are:

(a) The camera and microdensitometer advance mechanisms can produce small random variations in the position of each exposure on the film and hence the origin \vec{O} shifts randomly from frame to frame.

(b) No matter what method is used to find the exact center of a spot, there is an uncertainty in its position which reduces the accuracy of the values of \vec{a} , \vec{b} and \vec{O} . This can become a serious problem at energies far removed from the energy at which the vectors were originally determined.

(c) Naturally, the experimentalist attempts to minimize effects such as Moiré patterns, distortions due to camera or sample placement, screen shape, inhomogeneities in the phosphor screen or the film response and stray electric and magnetic fields. Nevertheless, these factors affect the position, shape and intensity of diffraction spots and must be taken into account.

It is therefore necessary to allow the algorithm to adjust the parameters \vec{a} , \vec{b} and \vec{O} at each energy to correct for the various fluctuations.

A.2. Operation

The computer program that we have developed uses the the following algorithm.

(1) Obtain three or more reliable positions $\vec{P}_{h,k,E}$ for intense spots at an energy close to the starting energy of the data. This can be done by manual inspection of a contour map of the photographic negative, cf. Fig. 9a.

(2) Index these spots and input the list of indices (but not coordinates) for all those beams whose I-V profiles are required.

(3) Calculate an optimal set of values for \vec{a} , \vec{b} and \vec{O} by a least-squares fit to the spot positions. The best values are those which minimize Δ , the

sum of the squares of the differences between the measured spot positions \vec{P} and the positions \vec{O} predicted from \vec{a} , \vec{b} and \vec{O} , cf. Fig. 9b:

$$\vec{Q}_{h,k,E} = \vec{O} + h\vec{a} + k\vec{b}, \quad (\text{A.1})$$

$$\vec{D}_{h,k,E} = \vec{Q}_{h,k,E} - \vec{P}_{h,k,E}, \quad (\text{A.2})$$

$$\Delta = \sum_{h,k} (\vec{D}_{h,k,E})^2. \quad (\text{A.3})$$

A linear three-variable regression (least-squares fit) is used at this stage to determine independently the x and y components of \vec{a} , \vec{b} and \vec{O} .

(4) The digitized data for a photographic frame at some beam energy E are now examined. Initially, E will be close to the beam energy used in (1) and subsequently it will be incremented on successive cycles until all the frames have been processed.

(4.1) The magnitudes of \vec{a} and \vec{b} are scaled to the energy E and a set of predicted positions $\vec{Q}_{h,k,E}$ is produced for the beams in the list provided in (2), using Eq. (A.1).

(4.2) A search is carried out for the actual spot positions. The best estimate of the actual position is given by

$$\vec{Q}_{h,k,E}^1 = \vec{Q}_{h,k,E} + \vec{D}_{h,k,E-\Delta E}. \quad (\text{A.4})$$

$\vec{D}_{h,k,E-\Delta E}$ is the difference vector between the actual spot position and that predicted from the previous frame at energy E-ΔE. It was minimized by optimizing \vec{a} , \vec{b} and \vec{O} and in general will be very small and randomly oriented. However, it is useful to take into account the problems mentioned in (c) above, which can cause systematic disturbances in the positions of some beams.

Locating the actual spot position and measuring its intensity are done in our program in several optional ways. Starting from the predicted position $\vec{Q}_{h,k,E}$, one can simply integrate the intensity within a region around that position, perform a background subtraction and denote the result as the beam intensity. The center of mass of the intensity is calculated and called the

actual beam position. The range of the integration is determined from a generous estimate of the half-width at half maximum of the diffraction features (in both the x and y directions) supplied by the operator. It should be large enough to include all of the beam intensity. The background is a simple average found from the transmission values along an ellipse (whose x and y axes are related to the x and y HWHM values of the spot) centered on the spot center. Alternatively, a sloping background found from the intensity on either side of the beam is subtracted.

Usually it is preferable to find the actual spot position before integration. The simplest approach is to find in the negative image the smallest intensity point in a region (the size of which is determined by the operator) around the predicted position and define this as the beam center. At high incident-beam energies or with small reciprocal unit cells this approach occasionally fails due to the possible presence of another more intense beam within the search area. If this is likely to be the case, the operator can specify for a search to be made for the nearest local intensity minimum.

(4.3) The cell vectors and origin are reoptimized using the actual spot positions $\vec{P}_{h,k,E}$. In most cases it is perfectly adequate to use the method in step (3); however, in complex cases it is useful to make the procedure more stable by constraining the parameters \vec{a} , \vec{b} and $\vec{0}$. This can be done in two ways. First, the operator can impose slack constraints by specifying the maximum percentage change with energy of these parameters. Second, strict constraints can be introduced which make use of known relationships between the parameters. For example, it may be that the magnitude $|\vec{a}|$ of \vec{a} and the magnitude $|\vec{b}|$ of \vec{b} are known to be in a constant ratio. Introducing this into the optimization can make the problem non-linear, but it has the advantage of simplifying the least-squares surface, and of thus making it more likely that undesired local

minima are avoided.

We have found it useful to introduce the option of different levels of constraints in the following progression:

(i) $|\vec{a}| = R|\vec{b}|$, where R is a fixed constant. The parameters to optimize are now O_x , O_y , θ_a , θ_b and $|\vec{a}|$, where θ_a and θ_b are the orientations of \vec{a} and \vec{b} with respect to the x axis.

(ii) Constraint (i) together with $\theta_a - \theta_b = \theta$, where θ is fixed. Now, O_x , O_y , θ_a and $|\vec{a}|$ remain to be determined.

(iii) Constraints (ii) together with $\theta_a = \theta_0$, where θ_0 is a constant. Only O_x , O_y and $|\vec{a}|$ remain free.

(iv) Finally, we can refrain from optimizing any of the parameters after the initial optimization in step (3).

The cycle in step (4) is continued until all the frames have been processed. Step (3) is performed only once.

The steps (1) and (2) are performed by the operator prior to running the program. They constitute the input to the program, together with a file containing the digitized data, an indication of the width of the diffraction features, a set of limits which the unit cell vectors should not exceed, validity limits for the spot parameters and some numbers to define which options are taken within the program. The (h,k) indices of all observable beams could be generated automatically, but an input list is preferred as this allows a reduced set to be examined if required. It also allows complete control over the choice of primitive unit cell used to index the beams and in particular no assumptions regarding the domain structure of the surface need be introduced.

A.3 Validity tests

An extensive set of internal tests is performed during program operation. Failure of any of these tests is flagged for later investigation. The failures

are of two types. Hard failures arise when the measured intensity and/or the position of the spot are found to be wrong. This may be due, for example, to the beam being half off or totally off the screen. Hard failures result in the beam intensity being set to zero, $\vec{D}_{h,k,E}$ is set to zero and the position of that beam is not used in the reoptimization of the cell vectors.

Soft failures are flagged when the spot is not reasonably close to its predicted position, the intensity is not significantly above the background, the width of the spot is suspiciously larger or smaller than expected (allowing the program to discriminate against flares on the screen or dust particles on the film) and the background is unreasonable. A soft failure is flagged as such; then the measured intensity is reported, but the spot position is not used in the reoptimization of the cell vectors. In all cases, therefore, the cell vectors are determined only from those beam positions which are not flagged and therefore are considered to be reliable.

A.4 Implementation

A modular suite of programs written in a fairly standard FORTRAN IV 1966 code are operating in a CDC 7600 environment. These programs should be easily transferable to other environments, with the following exceptions: the translation of the photographic data into a data file accessible to the program is generally installation-dependent; the non-linear optimization routine LSQNDN (from the NPL library) would have to be replaced if the NPL library is not locally available; similarly, graphical output uses the Berkeley-specific IDDS package and these routines would require replacement. The programs are available in combination with a Van Hove/Tong LEED program package, that includes dynamical LEED intensity calculation programs, R-factor programs and other ancillary programs.

At present the programs require an entire frame of data to be in high-

speed memory at any one time. This is not necessary and core requirements could be reduced by storing only those parts of a frame that are predicted to contain useful information. This would enable the programs to operate in a minicomputer environment. The programs are well suited to be used in conjunction with a video camera observing the LEED screen or with a digital position-sensitive detector replacing the LEED screen.

ACKNOWLEDGEMENTS

This work was supported by the Director, Office of Energy Research, Office of Basic Energy Sciences, Materials Sciences Division of the U.S. Department of Energy under Contract DE-AC03-76SF00098. We wish to thank Mr. Greg Lewis for his valuable assistance in the experimental analysis.

REFERENCES

1. A.M. Bradshaw, Surf. Sci. 80, 215 (1979).
2. H.H. Storck, N. Golumbic and R.B. Anderson, in "The Fischer-Tropsch and Related Reactions", Wiley (New York), 1951.
3. F.G. Dwyer, Catalysis Rev. 6, 261 (1972).
4. G.A. Somorjai, "Chemistry in Two Dimensions: Surfaces", Cornell University Press (Ithaca, New York) 1981, p. 196.
5. D.G. Castner, B.A. Sexton and G.A. Somorjai, Surf. Sci. 71, 519 (1978).
6. A.M. Bradshaw and F.M. Hoffmann, Surf. Sci. 72, 513 (1978).
- 7a. H. Ibach and D.L. Mills, "Electron Energy Loss Spectroscopy and Surface Vibrations", Academic Press (New York), 1982.
- 7b. L.H. Dubois and G.A. Somorjai, Surf. Sci. 91, 514 (1980).
8. R.J. Koestner, M.A. Van Hove and G.A. Somorjai, Surf. Sci. 107, 439 (1981).
9. S. Andersson and J.B. Pendry, Phys. Rev. Lett. 43, 363 (1979); J. Phys. C13, 3547 (1980).
10. M.A. Passler, A. Ignatiev, F. Jona, D.W. Jepsen and P.M. Marcus, Phys. Rev. Lett. 43, 360 (1979).

11. S.Y. Tong, A. Maldonado, C.H. Li and M.A. Van Hove, Surf. Sci. 94, 73 (1980).
12. R.J. Behm, K. Christmann, G. Ertl, M.A. Van Hove, P.A. Thiel and W.H. Weinberg, Surf. Sci. 88, L59 (1979); R.J. Behm, K. Christmann, G. Ertl and M.A. Van Hove, J. Chem. Phys. 73, 2984 (1980).
13. R.P. Eischens and W.A. Fliskin, Adv. Catalysis 10, 1 (1958).
14. P.A. Thiel, E.D. Williams, J.T. Yates, Jr. and W.H. Weinberg, Surf. Sci. 84, 54 (1979).
15. P.C. Stair, T.J. Kaminska, L.L. Kesmodel and G.A. Somorjai, Phys. Rev. B11, 623 (1975).
16. R.J. Koestner, M.A. Van Hove and G.A. Somorjai, Surf. Sci. 121, 321 (1982).
17. R.M. Lambert and C.M. Comrie, Surf. Sci. 38, 197 (1973).
- 18a. M.A. Van Hove and S.Y. Tong, "Surface Crystallography by LEED", Springer-Verlag (Heidelberg) 1979.
- 18b. M.A. Van Hove and G.A. Somorjai, Surf. Sci. 114, 171 (1982).
19. M.A. Van Hove and R.J. Koestner, in Proc. on Determination of Surface Structure by LEED, Plenum (New York) 1982.
20. E. Zanazzi and F. Jona, Surf. Sci. 62, 61 (1977).
21. J.B. Pendry, J. Phys. C13, 937 (1980).
22. J. Pritchard, Surf. Sci. 79, 231 (1979).
23. P. Chini, V. Longoni and V.G. Albano, Adv. Organomet. Chem. 14, 285 (1976).
24. G. Blyholder, J. Phys. Chem. 79, 756 (1975).
25. P. Hofmann, S.R. Bare, R. Brooks, N.V. Richardson and D.A. King, Inf. Quarterly for Surf. Sci. (SRC-Daresbury) 8, 2 (1981); R. Brooks, N.V. Richardson and D.A. King, Surf. Sci. 117, 434 (1982)
26. J.P. Biberian and M.A. Van Hove, Surf. Sci. 118, 443 (1982).
27. R. Destro and M. Simonetta, Acta Cryst. B33, 3219 (1977).
28. H. Vahrenkamp, Chem. Ber. 111, 3472 (1978).
29. R.W.G. Wyckoff, "Crystal Structures", Vol. 1, 2nd ed., Wiley (London) 1965; Structure Reports: Metals and Inorganic Sections, publ. for Int'l Un. of Cryst. by D. Reidel (Boston); and references therein.
30. W. Hoesler and W. Moritz, Surf. Sci. 117, 196 (1982).
31. P.C. Stair, Ph.D. Thesis, University of California, Berkeley (1977).

TABLE CAPTION

Table I. Structural parameter variations in the LEED calculations, following the labelling shown in Figure 1. The change in the tilt angle θ_{CO} (> 0 for tilt towards a bridged CO) is accompanied by simultaneous changes in $d_{\perp CC}$ and $d_{\parallel CC}$. The level of theoretical approximation is indicated as "kin" for kinematic limit, "part" for partial multiple scattering and "dyn" for full multiple scattering (see text for details). Parameter variations are given as "initial value (step) final value", indicating both the step size "step" and the range of variation which runs from "initial value" to "final value".

TABLE I

d_{LRhc} [Å]	d_{LCC} [Å]	d_{CO} [Å]	$d_{//CC}$ [Å]	θ_{CO} [°]	approx.
1.4 (0.1) 1.9	-0.05 (0.1) 0.65	1.15	2.8 (0.1) 3.1	-40 (10) 30	kin
1.4 (0.1) 1.9	-0.2 (0.1) 0.1 0.15 (0.05) 0.3 0.35 (0.1) 0.65	1.15	3.1	0	kin
1.2 (0.1) 1.7	0.35	1.15	2.35 (0.15) 2.8	0	kin
1.4 (0.1) 1.9	0.35	1.15	2.95 (0.15) 3.4	0	kin
1.4 (0.1) 1.9	0.35	0.95 (0.1) 1.25	3.1	0	kin
1.3 (0.1) 1.8	0.35	1.15	2.65 (0.1) 3.35	0	part
1.3 (0.1) 1.8	0.25	1.15	3.05 (0.1) 3.35	0	part
1.3 (0.1) 1.8	0.15	1.15	2.65 (0.15) 3.1	0	part
1.3 (0.1) 1.8	0.15 (0.1) 0.45	1.15	3.1	0	part
1.3 (0.1) 1.8	0.0 (0.1) 0.3	1.15	3.0	0	part
1.3 (0.1) 1.8	0.35	0.95 (0.1) 1.15	3.1	0	part
1.3 (0.1) 1.8	0.35	0.95 (0.1) 1.25	3.1	0	dyn
1.3 (0.1) 1.8	0.2	0.95 (0.1) 1.25	2.85	0	dyn
1.3 (0.1) 1.8	0.1	0.95 (0.1) 1.25	2.75	0	dyn
1.3 (0.1) 1.8	0.15	1.15	2.65 (0.15) 3.1	0	dyn
1.3 (0.1) 1.8	0.35	1.15	2.65 (0.15) 3.1	0	dyn
1.3 (0.1) 1.8	0.05 (0.1) 0.35	1.15	2.85	0	dyn
1.3 (0.1) 1.8	-0.05 (0.1) 0.65	1.15	2.8 (0.1) 3.5	-40 (10) 30	dyn
1.3 (0.1) 1.8	-0.20 (0.1) 0.50	1.15	2.55 (0.1) 3.25	-40 (10) 30	dyn
1.3 (0.1) 1.8	0.45	1.15	2.55 (0.1) 3.25	-40 (10) 30	dyn
1.3 (0.1) 1.8	0.35	1.15	2.55 (0.1) 3.25	-40 (10) 30	dyn

FIGURE CAPTIONS

- Figure 1: The Rh(111)(2x2)-3CO surface structure, showing its projections onto the surface plane (at bottom) and onto a mirror plane of the structure (at top); a (2x2) unit cell is outlined. Large circles represent Rh atoms, the dotted ones being outside the plane of the figure. Small dotted circles indicate C and O positions satisfying a hexagonal CO overlayer of coverage $3/4$ (one unit cell of which is outlined), while small full circles indicate the optimum positions found in this study (but leaving all CO axes perpendicular to the surface). The independent structural parameters are labelled and some of the optimum interatomic and interlayer distances are indicated.
- Figure 2: R-factor contour plots for variations of some of the structural parameters shown in Figure 1. The non-varied parameters in each panel take the values listed explicitly in the figure. The kinematic approximation is used in the overlayer. The contour levels are separated by 0.025 and refer to our five-R-factor average.
- Figure 3: As figure 2 with partial multiple scattering within the overlayer.
- Figure 4: As figure 2 with full multiple scattering within the overlayer.
- Figure 5: As figure 2 with full multiple scattering within the overlayer using the optimized structural parameters.
- Figure 6: Experimental (thick lines) and theoretical (thin lines) I-V curves for Rh(111)(2x2)-3CO for a few structures near the optimal surface structure results for two values of the Rh-C spacing ($d_{\perp RhC} = 1.5\text{\AA}$

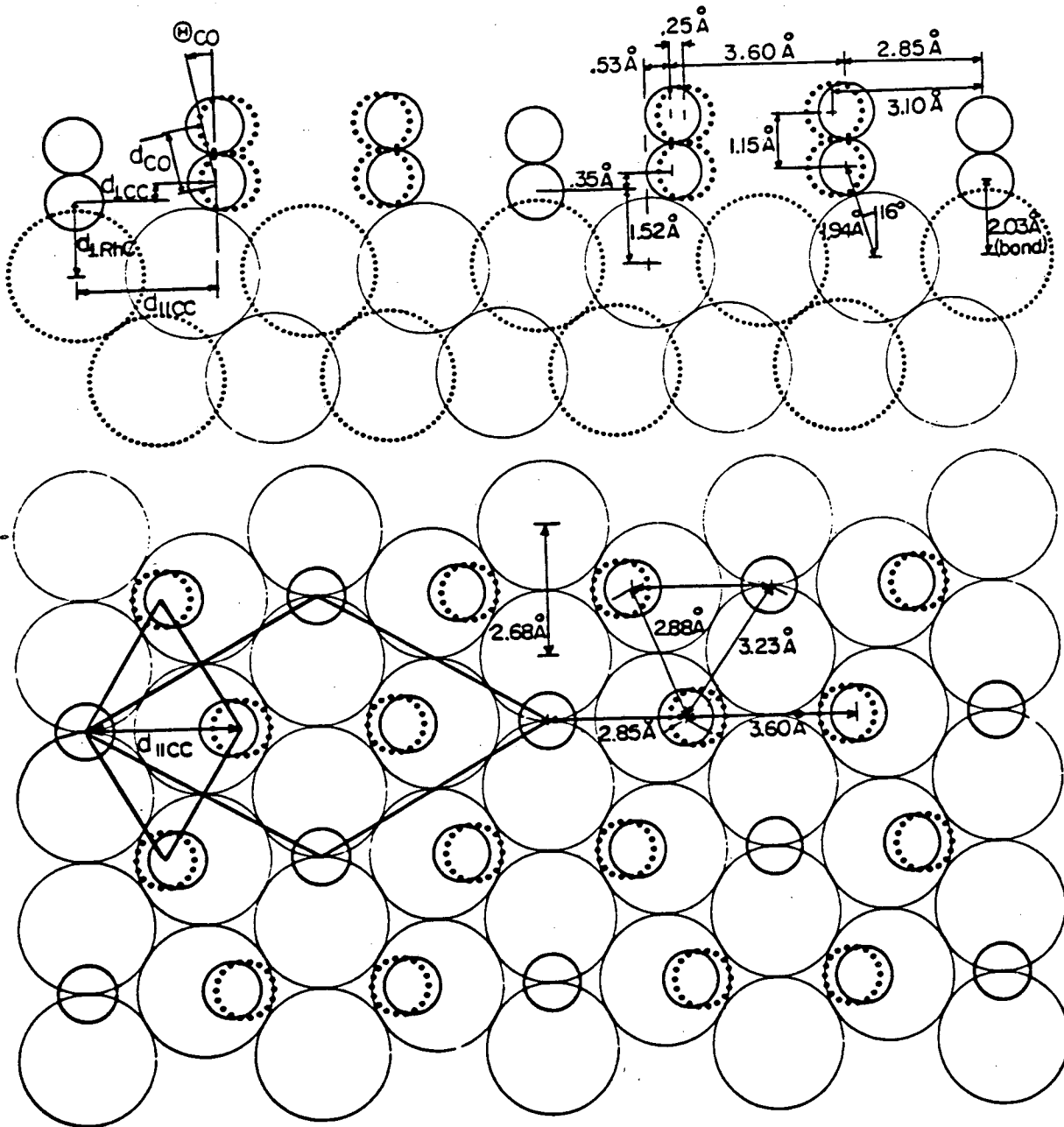
and 1.6Å) and two values of the CO tilt ($\theta_{CO} = 0$ and -10°) are shown; other parameters have the values $d_{\perp CC} = 0.35\text{Å}$, $d_{CO} = 1.15\text{Å}$ and $d_{\parallel CC} = 2.85\text{Å}$. Theoretical curves are shifted upwards for clarity.

Figure 7: Correlation of the effective carbon radius, r_C^{eff} defined as (metal-carbon bond length)-(bulk metal radius), with C-O bond length, d_{CO} , in metal carbonyl clusters and in CO adsorbed on surfaces at different bonding sites (top = terminal = linear, bridge = edge-bridging, hollow = face-bridging). The surface structures are obtained by LEED and are labelled by the crystallographic face and, for Rh, by the CO coverage.

Figure 8: Example of two interpretations of the same LEED pattern for a high coverage ($\theta = 0.6$) of CO on Cu(100). At this particular coverage, both models are commensurate with the substrate, producing a $c(5\sqrt{2} \times 5\sqrt{2})R45^\circ$ unit cell, indicated by dashed lines. Substrate atoms are drawn as open circles, CO molecules as filled circles. (a) Compressed hexagonal model: the unit cell of the overlayer alone is shown with full lines; a variety of adsorption sites exists. (b) Antiphase domain model: the domains consist of $c(2 \times 2)$ arrangements of CO molecules, separated by high-density boundaries; only one type of site appears in this structure, in agreement with vibrational loss measurements. (26)

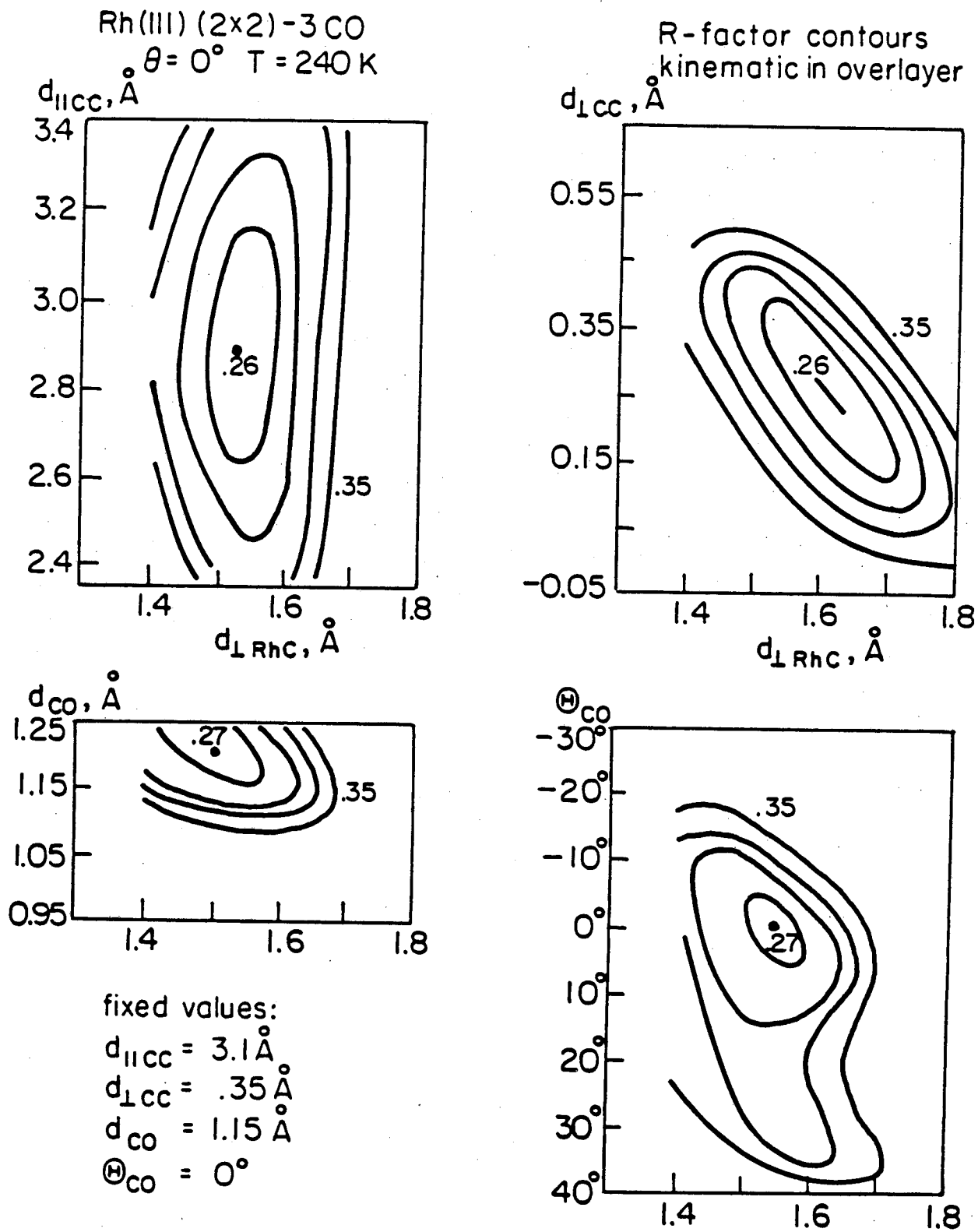
Figure 9: (a) Contour plot of the digitized photograph of a LEED pattern for Rh(111)(2×2)-3CO. The circular screen edge and the shadow of the sample holder can be recognized. (b) Indexing scheme for a general LEED pattern. The small circles represent actual spot positions, and the dots fitted spot positions.

Rh(III) (2x2) - 3 CO



XBL 828-6270

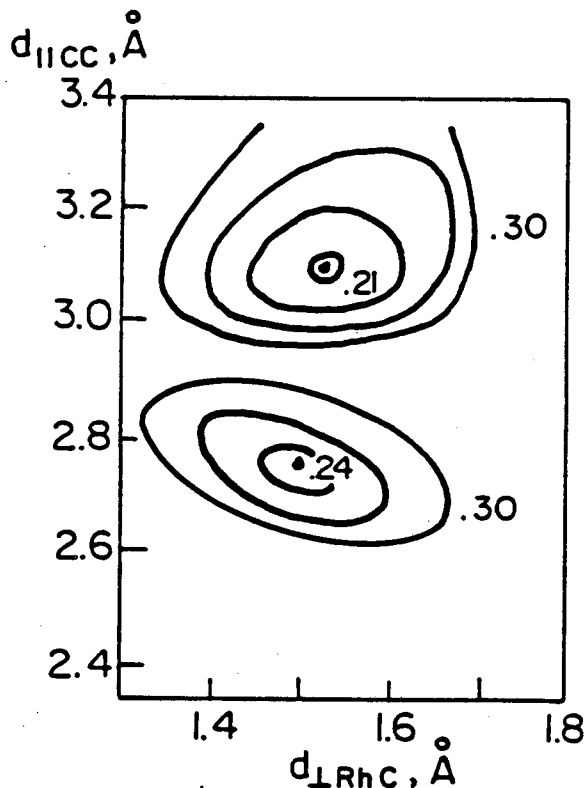
Figure 1



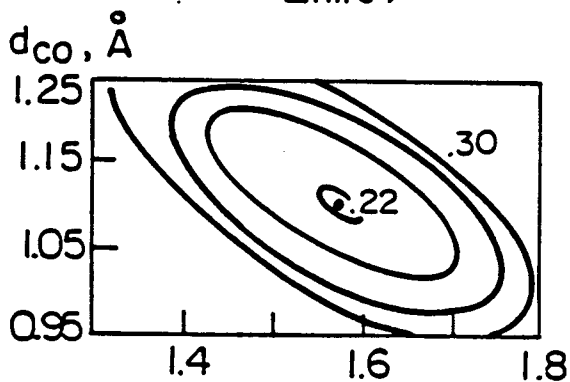
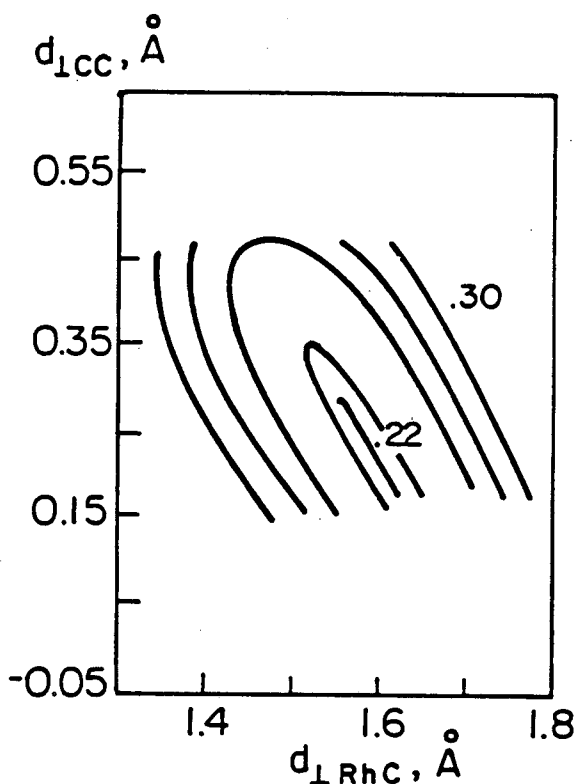
XBL 828-6274

Figure 2

Rh(III) (2x2) - 3 CO
 $\theta = 0^\circ$ T = 240 K



R-factor contours
dynamical in molecules



fixed values:

$$d_{\parallel cc} = 3.1 \text{\AA}$$

$$d_{\perp cc} = .35 \text{\AA}$$

$$d_{CO} = 1.15 \text{\AA}$$

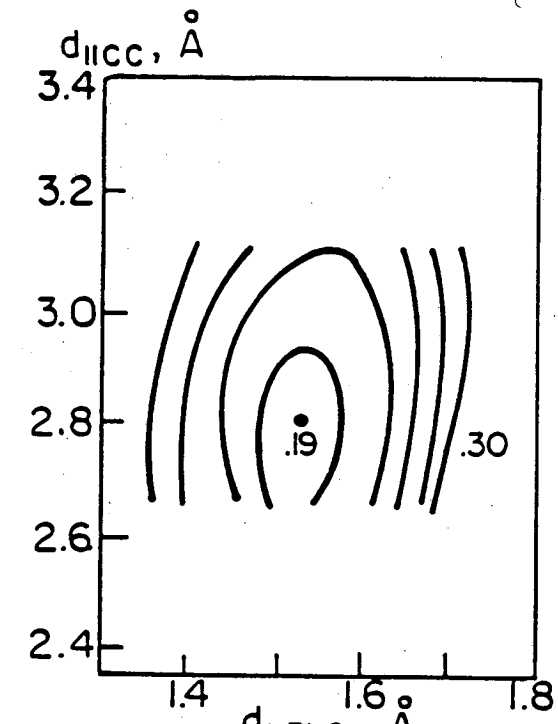
$$\theta_{CO} = 0^\circ$$

XBL 828-6273

Figure 3.

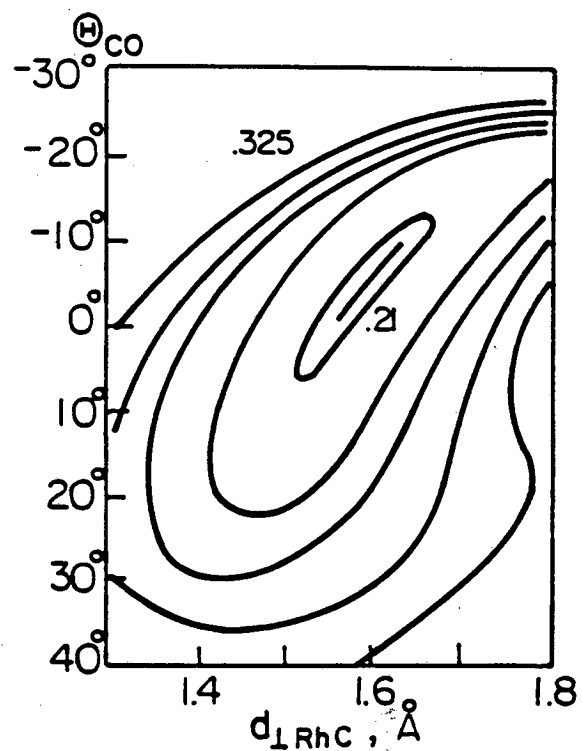
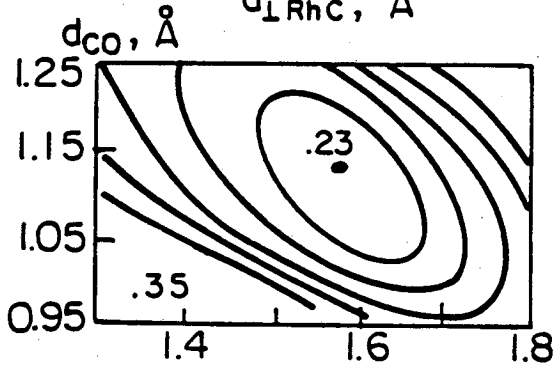
Rh(III)(2x2)-3CO
 $\theta = 0^\circ$ T=240K

R-factor contours
full dynamical



fixed values:

- $d_{\parallel cc} = 3.1 \text{ \AA}$
- $d_{\perp cc} = .35 \text{ \AA}$
- $d_{CO} = 1.15 \text{ \AA}$
- $\Theta_{CO} = 0^\circ$

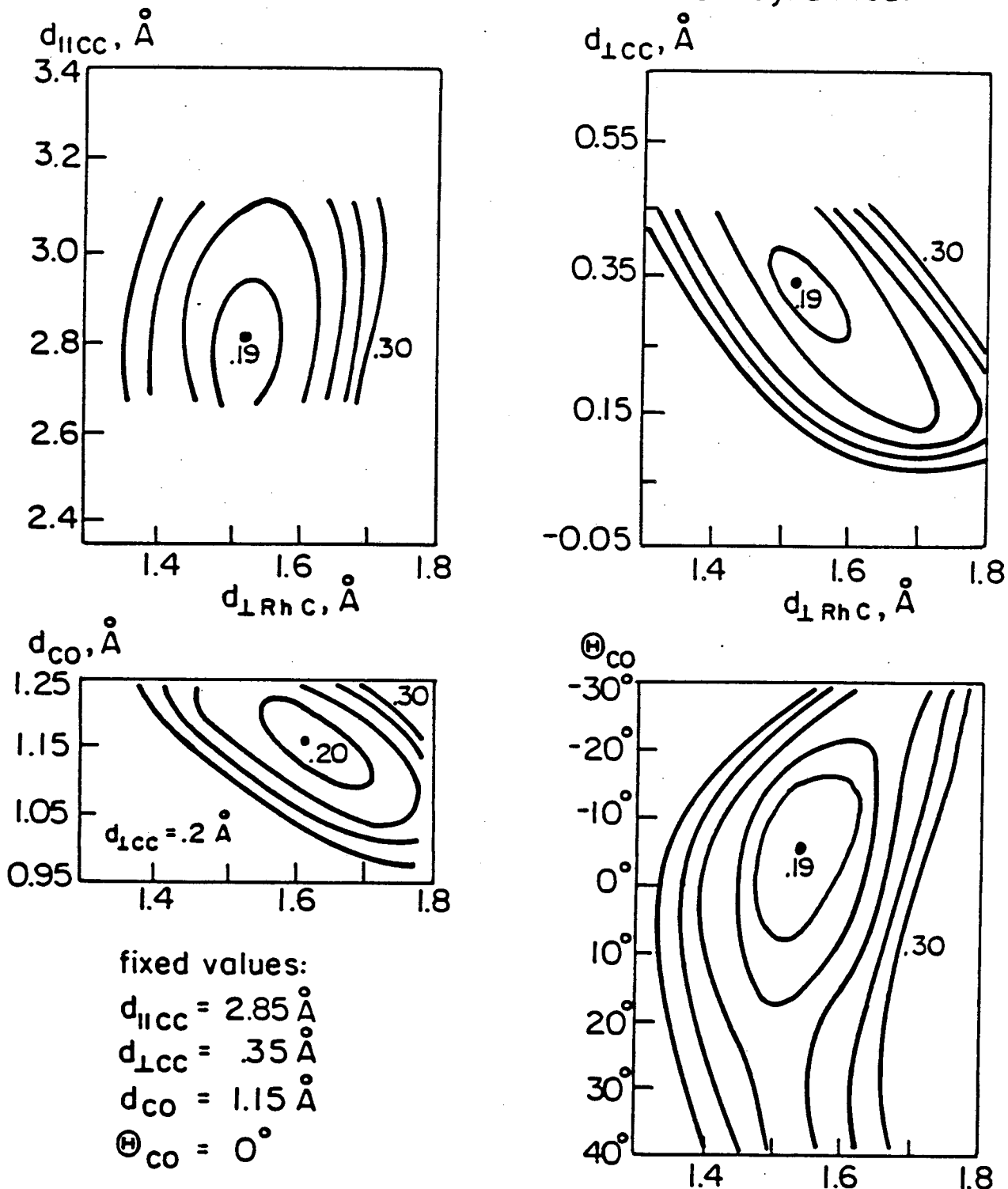


XBL 828-6272

Figure 4

Rh(III) (2x2) - 3 CO
 $\theta = 0^\circ$ T=240K

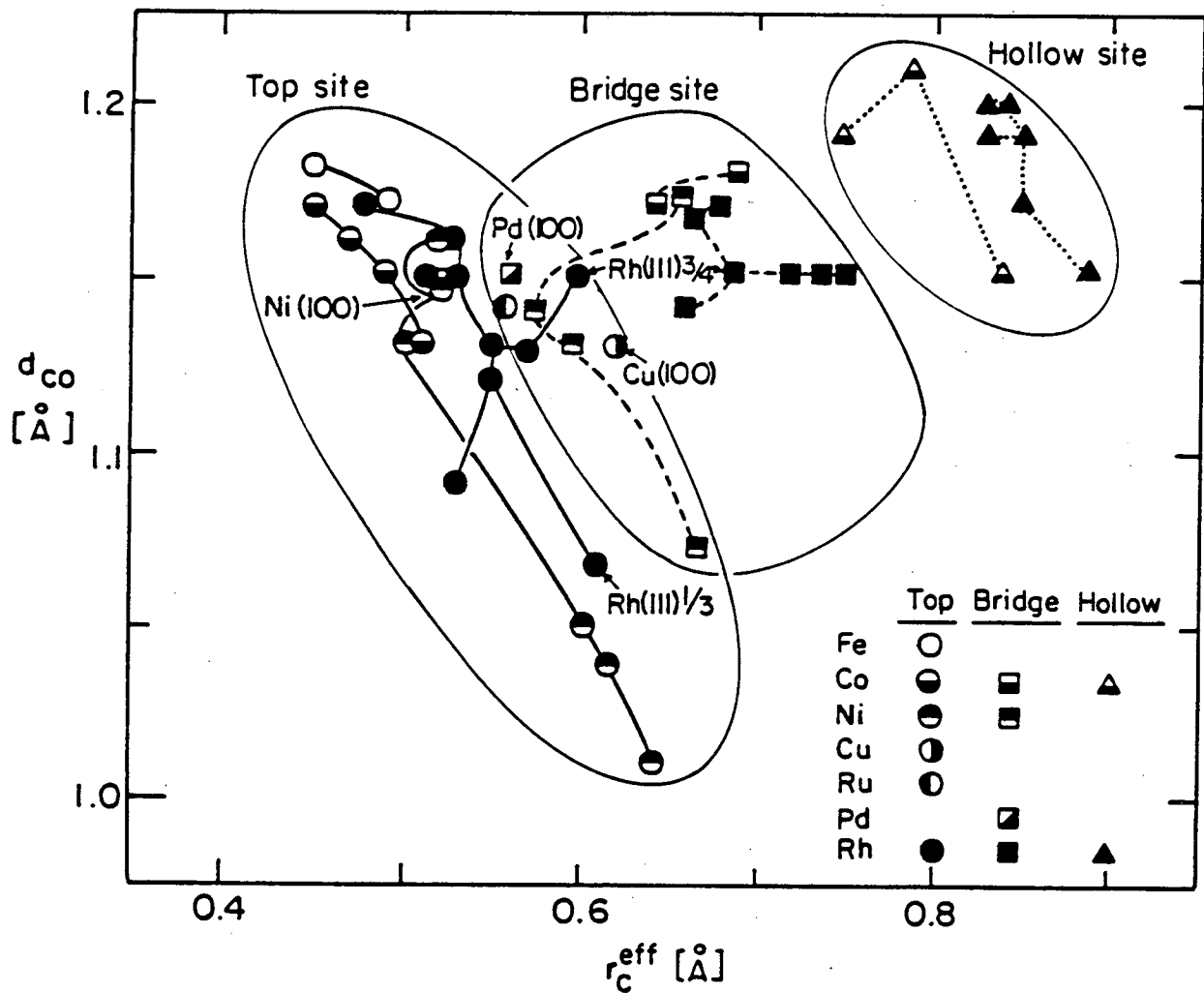
R-factor contours
full dynamical



XBL828-6275

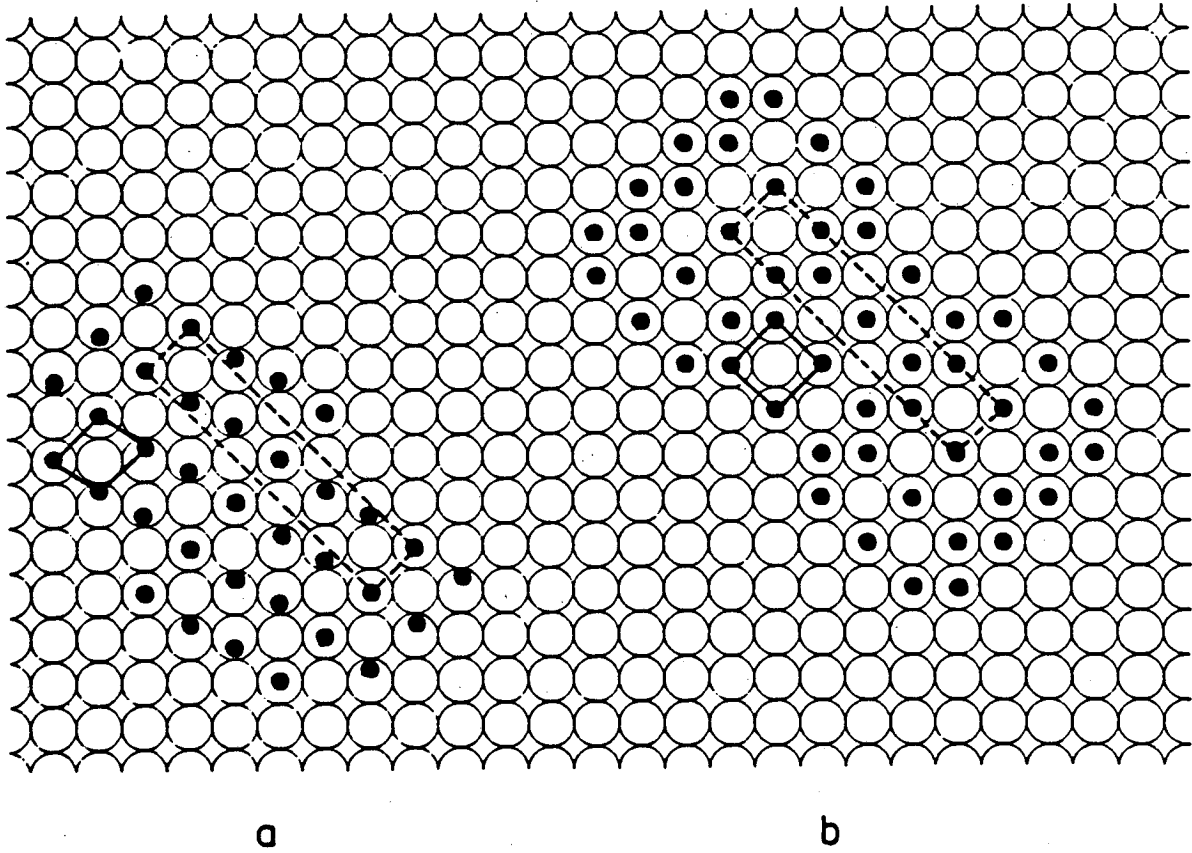
Figure 5

Metal-carbonyls: correlation of effective C radius in M-C bond with C-O bond length



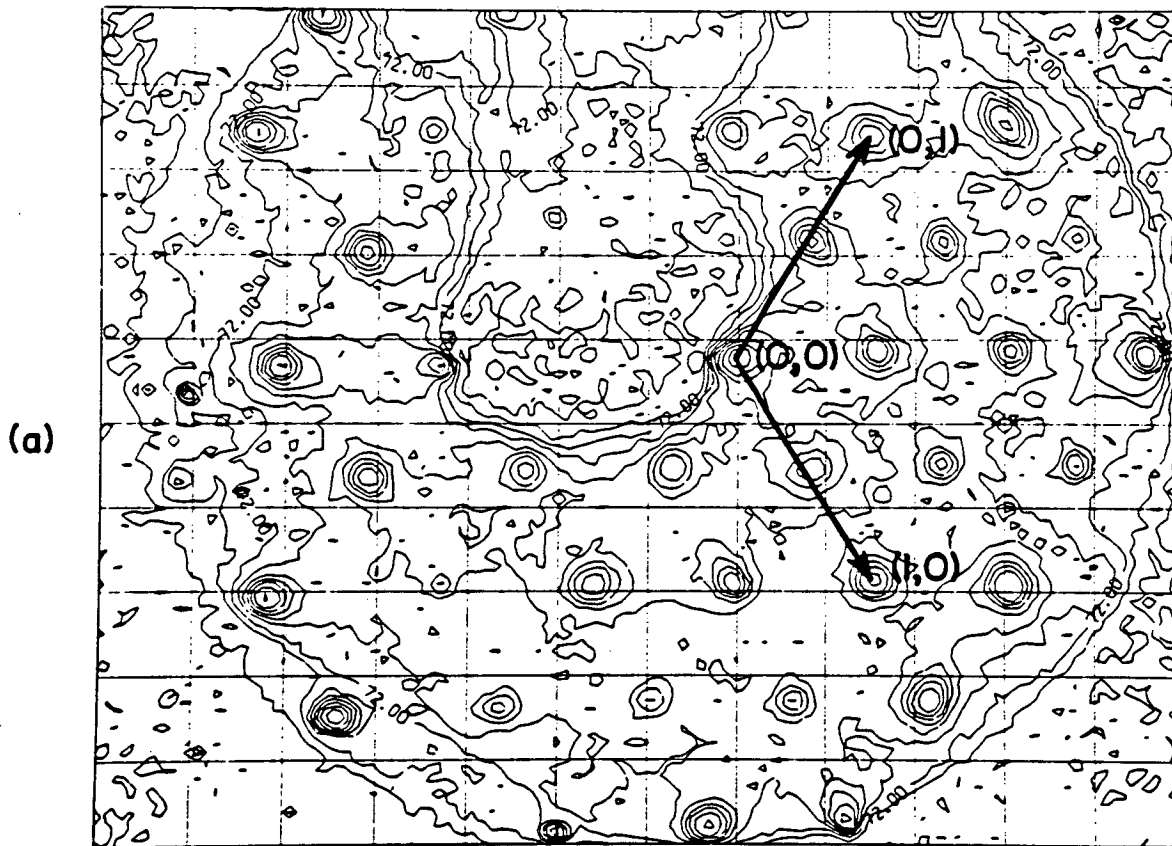
X BL 828-6271

Figure 7

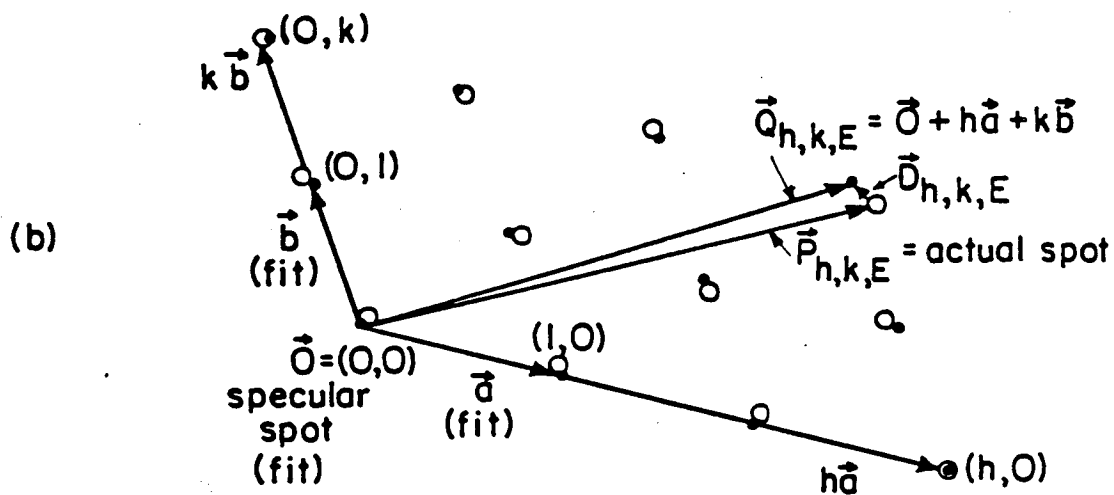


XBL 8212-12136

Figure 8



Rh(III) (2x2) - 3 CO, $(\theta, \phi) = (10^\circ, 0^\circ)$,
 $E = 144 \text{ eV}$



XBL 8211-3391

Figure 9

This report was done with support from the Department of Energy. Any conclusions or opinions expressed in this report represent solely those of the author(s) and not necessarily those of The Regents of the University of California, the Lawrence Berkeley Laboratory or the Department of Energy.

Reference to a company or product name does not imply approval or recommendation of the product by the University of California or the U.S. Department of Energy to the exclusion of others that may be suitable.

TECHNICAL INFORMATION DEPARTMENT
LAWRENCE BERKELEY LABORATORY
UNIVERSITY OF CALIFORNIA
BERKELEY, CALIFORNIA 94720